Redox-Dependent CO_2 Reduction Activity of CO Dehydrogenase from *Rhodospirillum rubrum*†

Jongyun Heo, Christopher R. Staples, and Paul W. Ludden*

From the Department of Biochemistry, College of Agricultural and Life Sciences, University of Wisconsin-Madison, Madison, Wisconsin 53706

Received November 6, 2000

ABSTRACT: Carbon monoxide dehydrogenase (CODH) from *Rhodospirillum rubrum* catalyzes both the oxidation of CO and the reduction of CO_2. Studies of the redox dependence of CO_2 reduction by *R. rubrum* CODH show that (1) CODH is unable to catalyze CO_2 reduction at potentials greater than −300 mV; (2) the maximum activity is observed at potentials less than −480 mV; and (3) the midpoint potential (E_m) of the transition from minimum to maximum CO_2 reduction activity occurs at ∼−339 mV. These results indicate that the C_{red1} state of *R. rubrum* CODH ($E_m = -110$ mV; $g_{zyx} = 2.03, 1.88, 1.71$) is not competent to reduce CO_2. Nernst analyses suggest that the reduction of CODH from the C_{red1} state to the CO_2-reducing form (C_{unc}, $g_{zyx} = 2.04, 1.93, 1.89$; $E < \sim -300$ mV) of the enzyme is a one-electron process. For the entire redox range, viologens stimulate CO_2 reduction by CODH more than 50-fold, and it is proposed that viologens accelerate the redox equilibration of redox buffers and $[Fe_4S_4]_B$ during catalysis.

INTRODUCTION

Carbon monoxide dehydrogenase (CODH)[1] from *Rhodospirillum rubrum* reversibly oxidizes CO to CO_2 according to the following scheme (*1*−*5*):

Scheme 1

$$CO + H_2O \rightleftharpoons CO_2 + 2H^+ + 2e^-$$

Recently, the general features of the *R. rubrum* CODH structure have become known by X-ray crystallography (*6*). The enzyme exists as a homodimer of the *cooS* gene product. The dimeric enzyme contains two C-clusters, two B-clusters, and a previously unknown cluster, referred to as the D-cluster, that bridges the two subunits. The arrangement of clusters in the enzyme is such that a C-cluster:B-cluster pair from opposite subunits are more proximal than the C-cluster and the B-cluster from a single subunit. The bridging D-cluster is most proximal to the B-clusters. The C-cluster serves as the active site for catalysis (*7*), and the assignment of the C-cluster in the crystal structure is based on its proximity to His265 and Cys531. CODHs with substitutions at these sites [e.g., H265V and C531A (*8*, *9*)] have greatly diminished CO oxidation activities and lack the spectroscopic signals attributed to the C-cluster. The B-cluster functions in electron transfer to CooF, the physiological electron acceptor of CODH (*10*), while the function of the D-cluster is not known. Further, there is not a spectroscopic signature for the D-cluster, although it must be represented in the published UV−vis and Mössbauer spectra.

We have proposed that CODH contains a C-cluster comprised of a [FeNi] binuclear subcluster (*7*, *9*, *11*, *12*). The [FeNi] binuclear subcluster is proposed to be bridged to a slow-relaxing (EPR properties) Fe-containing subcluster component that we refer to as FeS_C (formerly, FeS_C was referred to as $[Fe_4S_4]_C$) (*7*, *9*, *11*, *12*). Also proposed to be present based upon spectroscopic properties is a typical all-cysteinyl liganded $[Fe_4S_4]$ cluster that we termed $[Fe_4S_4]_B$ (*7*, *9*, *11*, *12*). In addition, a CO ligand (CO_L) has been detected, and based upon its presence in Ni-deficient CODH, it is believed to be bound to the Fe site of the putative [FeNi] cluster (*13*).

The route of intramolecular electron transfer following CO oxidation has been a matter of speculation for some time. Upon the basis of spectroscopic data, we have proposed three different redox states of the putative active site [FeNi] cluster: a fully oxidized state, $[(CO_L)Fe^{2+}\text{-}Ni^{2+}]^{4+}$; a one-electron-reduced state, $[(CO_L)Fe^{3+}\text{-}Ni^{2+}\text{-}H^-]^{4+}$; and a two-electron-reduced state, $[(CO_L)Fe^{2+}\text{-}Ni^{2+}\text{-}H^-]^{3+}$ (*11*). The redox states of the FeS_C and $[Fe_4S_4]_B$ clusters also have been established by UV−vis and EPR spectroscopy. FeS_C undergoes a reversible one-electron (2+/1+) redox step with a midpoint at −110 mV, and $[Fe_4S_4]_B$ undergoes a reversible one-electron (2+/1+) redox step with a midpoint at −418 mV (*7*, *12*). The following redox states of the [FeNi] cluster, FeS_C and $[Fe_4S_4]_B$ were proposed after analysis of CODH poised at the given potentials: (a) at potential (E) > −60 mV, all clusters are fully oxidized and EPR unobservable in

† Work described here was supported by Grant DE-FG02-87ER13691 (DOE Basic Energy Sciences program) to P.W.L. and by National Institutes of Health Grant 5F32 GM 19716 to C.R.S.

* To whom correspondence should be addressed. Phone: (608) 262-6859. Fax: (608) 262-3453. E-mail: pludden@cals.wisc.edu.

[1] Abbreviations: CODH, carbon monoxide dehydrogenase; EPR, electron paramagnetic resonance; E_m, midpoint potential; E_d, established redox potential; CN^-, cyanide; MOPS, 3-(*N*-morpholino) propanesulfonic acid; DTH, sodium dithionite; BSA, bovine serum albumin; MB, methylene blue; BV, benzyl viologen; MV, methyl viologen; SHE, standard hydrogen electrode; IC, indigo carmine; EDTA, ethylenediaminetetraacetic acid; Hb, bovine hemoglobin; DE-52, diethylaminoethyl cellulose; K_m, Michaelis constant; V_{max}, maximum activity; ACS, acetyl-CoA synthase.

10.1021/bi002554k CCC: $20.00
Published on Web 05/30/2001

perpendicular mode (i.e., $[(CO_L)Fe^{2+}\text{-}Ni^{2+}]^{4+}$, FeS_C^{2+}, and $[Fe_4S_4]_B^{2+}$); (b) at a calculated $E = -295$ mV, one-electron-reduced [FeNi] and FeS_C clusters, and oxidized $[Fe_4S_4]_B$ were proposed to be present: $[(CO_L)Fe^{3+}\text{-}Ni^{2+}\text{-}H^-]^{4+}$ was suggested to couple with FeS_C^{1+} to produce the EPR signal, C_{red1}, "g_{zyx}" = 2.03, 1.88, 1.71; (c) at a calculated $E = -326$ mV, a two-electron-reduced [FeNi] cluster, one-electron reduced FeS_C, and oxidized $[Fe_4S_4]_B$ were proposed to be present: "uncoupled state (C_{unc})" of FeS_C^{1+} as $[(CO_L)Fe^{2+}\text{-}Ni^{2+}\text{-}H^-]^{3+}$ is $S = 0$; (d) an addition of physiological substrate CO_2 (as a form of $NaHCO_3$) to the uncoupled state, a fully oxidized [FeNi] cluster and one-electron reduced FeS_C were proposed to be present: $[(CO_L)Fe^{2+}\text{-}Ni^{2+}]^{4+}$ was suggested to couple with FeS_C^{1+} to produce the EPR signal, C_{red2B}; and (e) at $E = -500$ mV, $[Fe_4S_4]_B$ was proposed to be reduced in addition to a fully reduced [FeNi] cluster and FeS_C: $[Fe_4S_4]_B^{1+}$ was suggested to couple with FeS_C^{1+} to produce the fast-relaxing EPR signal, C_{red2A} (*11*).

The experimental results presented here provide evidence that (i) CODH in the C_{unc} state can reduce CO_2 while CODH in the C_{red1} state cannot, and (ii) CODH in the C_{unc} state is one electron more reduced than CODH in the C_{red1} state.

MATERIALS AND METHODS

All preparations were performed in an anaerobic glovebox (Vacuum Atmospheres Dri-Lab glovebox model HE-493; O_2 < 2 ppm) unless otherwise noted. All columns were preequilibrated with an appropriate buffer prior to use.

Preparation of Redox-Dyes and Other Solutions. The buffers used for pH 7.5 and pH 8.5 were 100 mM MOPS (3-(*N*-morpholino) propanesulfonic acid, USB) and 100 mM TrisHCl (Tris (Hydroxymethyl) Aminomethane, Fisher), respectively. Thionin ($E_m^{\circ\prime} = +64$ mV versus SHE, Aldrich), methylene blue (MB, $E_m^{\circ\prime} = +11$ mV versus SHE, Allied Chemical), indigo carmine ($E_m^{\circ\prime} = -125$ mV versus SHE, Sigma), 2-hydroxy-1,4-naphthoquinone ($E_m^{\circ\prime} = -145$ mV versus SHE, Aldrich), phenosafranin ($E_m^{\circ\prime} = -252$ mV versus SHE, Aldrich), neutral red ($E_m^{\circ\prime} = -325$ mV versus SHE, Sigma), benzyl viologen (BV, $E_m^{\circ\prime} = -350$ mV versus SHE, Sigma), methyl viologen (MV, $E_m^{\circ\prime} = -457$ mV versus SHE, Aldrich), and sodium dithionite (DTH, $E_m^{\circ\prime} = \sim -500$ mV versus SHE, Fluka) were prepared in either MOPS or Tris-HCl buffer. $NaHCO_3$ (Fisher) was prepared in 1 M of either MOPS or TrisHCl buffer to avoid a pH shift.

Cell Growth. Wild-type *R. rubrum* Strain UR2 was cultured as described previously (*1*, *14*, *15*).

Purification of CODH. CODH was purified by a modification of our published protocol (*2*). This protocol involved addition of glycerol (5%) before heat treatment to protect the heat-labile Fe (*13*).

Preparation of CODH Samples. For the oxidation of CODH, as-isolated CODH (in MOPS buffer containing 2 mM DTH) was loaded onto a DE-52 column (0.5 cm × 1 cm, Whatman), and excess thionin was applied. Thionin was removed by washing with excess MOPS buffer. Oxidized CODH was eluted with MOPS buffer containing 0.2 M NaCl and was immediately passed through a Sephadex G-25 (0.5 cm × 15 cm, Pharmacia) gel filtration column to remove the NaCl.

CO_2 Reduction Assays. CO_2 reduction to CO by CODH was monitored by the spectrophotometric absorbance change observed upon the binding of CO product to reduced bovine hemoglobin (Hb; i.e., a shift of the Soret band from 433 to 419 nm) (*3*). The apparent initial rate of CO_2 reduction in the presence or absence of Hb has been shown to be the same (*3*), indicating that the initial rate of the measured CO_2 reduction (within 1 min) in the presence of Hb will not be skewed. Therefore, the irreversible formation of a carbonyl-hemoglobin (Hb-CO) complex during CO_2 reduction does not disturb the kinetic parameters of the described experiments on the given time scale.

The CO_2 reduction assay mixture (4 mL) contained 0.1 mM redox dye, 0.2 mg/mL Hb, and 0.9% NaCl in either 100 mM MOPS or 100 mM TrisHCl buffer. Anaerobic assay mixtures were prepared in cuvettes in the Vacuum Atmospheres glovebox and cuvettes were serum-stoppered before removal from the glovebox. Desired redox states of the assay mixture were obtained by adding concentrated DTH while monitoring changes in the extinction coefficient (ϵ) at the appropriate wavelength (λ_{max}) of the employed redox mediator in the assay mixture. Spectra were recorded on a Shimadzu model 1605 dual beam spectrophotometer. Since an excess of redox dye (0.1 mM final concentration) was employed for each experiment, the predetermined redox states of the assay mixtures were assumed to be maintained during the assay periods (0−1 min). 2-Hydroxy-1,4-naphthoquinone [$\lambda_{max} = 449$ nm (oxidized), $\epsilon = 1.5$ mM cm^{-1}] was employed to poise the assay mixtures at a potential of −295 mV (pH 8.5); phenosafranin [$\lambda_{max} = 518$ nm (oxidized), $\epsilon = 25.7$ mM cm^{-1}] was used to maintain a solution potential of −326 mV (pH 7.5). To conduct CO_2 reduction assays in the redox range 0 to −530 mV with a fixed pH 7.5, the following redox dyes were employed: (a) indigo carmine [$\lambda_{max} = 610$ nm (oxidized), $\epsilon = 19.9$ mM cm^{-1}], −50 through −156 mV; (b) 2-hydroxy-1,4-naphthoquinone, −160 through −210 mV; (c) phenosafranin, −210 through −300 mV; (d) neutral red [$\lambda_{max} = 521$ nm (oxidized), $\epsilon = 16.8$ mM cm^{-1}], −300 through −500 mV; and (e) DTH, −500 mV. While the main absorption peak of each dye is remote from the Soret peak (419 nm) of Hb-CO, there is still significant absorption of the dyes in the 419 nm region. Combining all dyes in one assay solution accumulatively overwhelms the absorption at Soret peak (419 nm). Therefore, a single redox dye was used for the appropriate potential range. At all pHs (pH 7.5 and 8.5) and potentials (0 to −530 mV) assayed, Hb (Sigma, $E_m = +102$ mV) was fully reduced. The one-electron mediators MB [$\lambda_{max} = 664$ nm (oxidized), $\epsilon = 59.9$ mM cm^{-1}], MV [$\lambda_{max} = 601$ nm (reduced), $\epsilon = 9.7$ mM cm^{-1}] or BV [$\lambda_{max} = 599$ nm (reduced), $\epsilon = 9.3$ mM cm^{-1}] had no effect on the formation of Hb-CO. CO_2 reduction activities are expressed as μmol CO-formed min^{-1} mg^{-1} protein (specific activity) (*3*).

For experiments presented in Table 1, the assay mixture for CO_2 reduction assays at estimated redox potentials (E_d) ≥ −295 mV contained 150 μM CODH, 0.1 mM 95% reduced 2-hydroxy-1,4-naphthoquinone ($E_d = -295$ mV), 0.2 mg/mL Hb, and 0.9% NaCl in either 100 mM TrisHCl or 100 mM MOPS buffer. CO_2 reductions were

Table 1: Quantification of the Apparent CO_2 Reduction Rate at Various Redox States of CODH

	reduced clusters[b](%)		one-electron mediator			
E_d[a] (mV)	$-CO_2$	$+CO_2$	MB[c]	BV[d]	MV[e]	specific activity[f]
+64	0	0	−	−	−	0
(pH 7.5)			+	−	−	ND[g]
			−	+	−	ND
			−	−	+	0
−120	ND	ND	−	−	−	0
(pH 7.5)			+	−	−	ND
			−	+	−	ND
			−	−	+	0
−295	49	49	−	−	−	$(8.5 \times 10^{-5}) \pm (2.3 \times 10^{-6})$
(pH 8.5)	48	49	+	−	−	$(9.4 \times 10^{-5}) \pm (8.8 \times 10^{-6})$
	48	49	−	+	−	$(9.9 \times 10^{-5}) \pm (6.3 \times 10^{-6})$
	49	49	−	−	+	$(9.4 \times 10^{-5}) \pm (1.6 \times 10^{-6})$
−295	50	49	-	−	−	$(4.2 \times 10^{-5}) \pm (8.9 \times 10^{-6})$
(pH 7.5)	49	49	+	−	−	$(8.5 \times 10^{-5}) \pm (2.4 \times 10^{-6})$
	48	48	−	+	−	$(6.0 \times 10^{-5}) \pm (7.9 \times 10^{-6})$
	49	49	−	−	+	$(5.2 \times 10^{-5}) \pm (4.4 \times 10^{-6})$
−326	51	50	−	−	−	$(1.6 \times 10^{-1}) \pm (3.2 \times 10^{-2})$
(pH 7.5)	50	50	+	−	−	$(2.0 \times 10^{-1}) \pm (8.2 \times 10^{-2})$
	49	49	−	+	−	$(1.2 \pm 6.7) \times 10^{-3}$
	49	48	−	−	+	$(1.0 \pm 2.2) \times 10^{-2}$
−500	100	103	−	−	−	$(2.3 \times 10^{-1}) \pm (7.8 \times 10^{-2})$
(pH 7.5)	100	102	+	−	−	$(3.0 \times 10^{-1}) \pm (3.1 \times 10^{-2})$
	100	101	−	+	−	$(9.4 \pm 4.6) \times 10^{-3}$
	99	99	−	−	+	$(1.1 \times 10^{1}) \pm (3.3 \times 10^{-3})$

[a] Estimated redox potentials. [b] Percent reduced UV-observable metal clusters in the absence of $NaHCO_3$ ($-CO_2$) and in the presence of $NaHCO_3$ (10 mM, $+CO_2$). The estimation of the percentage of reduced-metal clusters monitored at 420 nm was described in the Materials and Methods. [c] MB, methylene blue. [d] BV, benzyl viologen. [e] MV, methyl viologen. [f] Apparent CO_2 reduction activities are expressed as μmol CO-formed min^{-1} mg^{-1} protein). [g] Not determined. CO_2 reduction was assayed by monitoring the conversion rate of hemoglobin (Hb) to carboxyhemoglobin (Hb-CO) in the presence of CODH and $NaHCO_3$ (a source of CO_2) as described in the Materials and Methods.

initiated by adding $NaHCO_3$ to a final concentration of 50 mM to the assay mixture, and CO_2 reduction rates were monitored by the change in UV-absorption spectra of the Soret peak at 419 nm due to accumulation of Hb-CO for 1 min. All of the CO_2 reduction rates (slopes) were linear for 1 min with $R^2 > 0.9998$. Notice that high concentrations of CODH (150 μM) and $NaHCO_3$ (50 mM) were required to observe CO_2 reduction at this redox potential. Therefore, CODH was added to these assay mixtures before poising the assay mixture to the desired redox potential. Furthermore, titration of the assay mixture containing CODH with a commercial DTH which contained a significant amount of Na_2CO_3 did not affect the quantification of the CO_2 reduction rate because an excess amount of both $NaHCO_3$ and CODH were required for the CO_2 reduction in this potential range.

For the measurement of CO_2 reduction at low potentials ($E_d \leq -326$ mV), the assay mixture (10 mM $NaHCO_3$, 0.2 mg/mL Hb, and 0.9% NaCl in 100 mM MOPS) was poised with either 0.1 mM 99% reduced phenosafranin or 2 mM DTH. For these assays, CO_2 reduction was initiated by the addition of 0.15 μM CODH to the assay cuvette (note: 10000-fold lower amount of CODH, and 5-fold less $NaHCO_3$ were used in assays at lower potential). The effect of one-electron mediators (MB, BV, and MV) was tested by adding each mediator (50 μM final concentration) to the assay system prior to initiating the reaction. All CO_2 reduction activity measurements were repeated 10 times to obtain quantitative data.

Protein Assays. The CODH samples were determined to be greater than 95% pure by SDS−PAGE analysis. CODH concentrations were determined colorimetrically using bovine serum albumin (BSA, Sigma) as a standard (*16*). BSA solution was standardized against carbonic anhydrase prior to use.

UV−Vis Absorption Spectra. As-isolated CODH was loaded onto a DE-52 column (0.5 cm × 1 cm). Excess thionin was passed over the bound protein, then washed off by passage of several column volumes of either 100 mM MOPS or 100 mM TrisHCl buffer. The protein was eluted with 200 mM NaCl in either 100 mM of MOPS or TrisHCl buffer. To poise the samples at the desired potentials, an excess of one of the indicated redox dyes (0.5 mL of 5 mM), [either 99% reduced 2-hydroxy-1,4-naphthoquinone (for −295 mV, pH 8.5 mV), or 86% reduced phenosafranin (for −295 mV, pH 7.5), or 95% reduced phenosafranin (for −326 mV, pH 7.5)] was added to each thionin-oxidized CODH sample (0.2 mL of 0.2 mM). Redox mediators were removed by passing the samples down a Sephadex G-25 column (0.5 cm × 5 cm, Pharmacia), and eluents were transferred immediately to serum-stoppered quartz cuvettes. Spectra for UV-observable metal clusters at different redox states were measured at 420 nm within 1 min. After recording the spectrum of a sample at the desired redox potential, both $NaHCO_3$ (10 mM final concentration) and one-electron mediator (either MB, BV, or MV; 50 μM final concentration) were introduced anaerobically and the spectrum was immediately recorded. The UV−vis absorption spectra obtained using this method have a certain degree of inherent error, but can be generally used to assess the amount of oxidized/reduced clusters present if the spectra are recorded within 1 min.

For Table 1, the fraction of reduced-metal clusters at different redox states was estimated by comparison of these spectra to those of samples treated with HCO_3^--free DTH (defined as 100% reduced) and samples oxidized with thionin

(defined as fully oxidized, i.e., 0% reduced). The extinction coefficients of thionin-oxidized and DTH-reduced CODH samples were 33.5 and 17.9 mM^{-1} cm^{-1}, respectively, in agreement with previous results (*1*, *14*).

Nernst Analyses of CO_2 Reduction Activity. The CODH-dependent rate of CO_2 reduction was determined as a function of redox potential. The resulting data plot was fitted to a Boltzmann sigmoidal curve and modeled as a redox-dependent reaction using the Nernst equation (eq 1).

$$E_d = E_m - \frac{RT}{nF} \ln \frac{[CODH^a]}{[CODH^i]} \quad (1)$$

This model assumes that active ($CODH^a$) and inactive ($CODH^i$) forms of CODH correspond to different redox states of the enzyme. The calculated solution potential is given as an established redox potential (E_d). The rate of CO_2 reduction by CODH can be expressed as a fraction of active CODH for CO_2 reduction (γ_a) as shown in eq 2.

$$\text{Fraction of } CO_2 \text{ reduction activity} \equiv \gamma_a = \frac{[CODH^a]}{[CODH^i] + [CODH^a]} \quad (2)$$

Rearrangement of eq 1 and combination with eq 2 yields eq 3.

$$\gamma_a = \frac{1}{1 + e^{-nF(E_m - E_d)/RT}} \quad (3)$$

Data were plotted as γ_a versus E_d, and the theoretical curves were fitted to eq 3 using the GraphPad Prism version 3.00 (GraphPad Software Incorporated). The values for n and E_m were determined by fitting curves to eq 3.

Data Analyses. In this study, the values and the corresponding standard errors presented were calculated from the best fit of the data normalized to the protein concentrations.

RESULTS AND DISCUSSION

CO_2 Reduction Rate versus the Solution Potential. Table 1 and Figure 1A show the rates of CO_2 reduction at various conditions of redox, pH, and electron donor. As seen in Table 1 and Figure 1A, CODH is inactive with respect to CO_2 reduction when the enzyme is fully oxidized (+64 mV) or at the midpoint of the C_{red1} state (−110 mV) (*7*, *12*). The most important result of this set of experiments is that the enzyme goes from being essentially inactive to being fully active for CO_2 reduction as the redox potential of the assay mixture is lowered to −400 mV (Figure 1).

Redox-Dependent CO_2 Reduction Rates and a UV−Vis Unobservable Redox Event over the Potential Range −200 to −340 mV. At −295 mV, a trace of CO_2 reduction activity is observed at both pH 8.5 and pH 7.5 (Table 1). At this potential, the C_{red1} EPR signal is fully developed (i.e., FeS_C is reduced but $[Fe_4S_4]_B$ is oxidized, as described previously) (*11*). Upon lowering the redox potential to −326 mV, the rate of CO_2 reduction by CODH increases approximately 2000-fold. Note that both 1000-fold more enzyme and a 5-fold higher $NaHCO_3$ concentration are included in the assays at −295 mV compared to the assays at −326 mV. In contrast to the drastic increase in CO_2 reduction rate caused by lowering the potential from −295 to −326 mV, the UV−vis spectrum of CODH is virtually unchanged (Table 1). This finding is consistent with previously reported data (*7*, *12*).

To further analyze the redox dependence of the catalytic activity of CODH while minimizing the effect of reduced $[Fe_4S_4]_B$, the apparent CO_2 reduction rates at pH 7.5 within a narrow redox range (−200 to −340 mV) were measured quantitatively (Figure 1A, trace I). Figure 1A trace I shows that the transition of inactive to active CODH for CO_2 reduction is an $n = \sim 1$ process with an E_m of ∼−339 mV.

Because the redox event of each cluster is a one-electron process with midpoint potentials (E_m) of FeS_C ($E_m = -110$ mV) and $[Fe_4S_4]_B$ ($E_m = -418$ mV) (*7*, *12*), the proportion of reduced clusters can be calculated. The estimated fractions of reduced FeS_C using eq 2 are 99.92% at $E_d = -295$ mV and 99.98% at $E_d = -326$ mV, indicating that the proportion of reduced FeS_C is essentially unchanged by lowering the E_d from −295 to −326 mV. Similarly, the increase in the percentage of reduced $[Fe_4S_4]_B$ upon a decrease in potential from −295 to −326 mV is minor. At −295 mV, 0.85% of $[Fe_4S_4]_B$ is calculated to be reduced and at −326 mV, 2.77% of $[Fe_4S_4]_B$ is calculated to be reduced. Even after compensating for the possible effect of reduced $[Fe_4S_4]_B$, an approximately 600-fold increase in the CO_2 reduction rate is still observed upon lowering the potential from −295 to −326 mV.

Lowering the redox potential from −326 to −500 mV further increases the CO_2 reduction rate by 1.51-fold while the calculated fold-increase of reduced $[Fe_4S_4]_B$ is 35-fold (3% at $E_d = -326$ mV, and 96% at $E_d = -500$ mV) (Table 1). There is no significant effect of CO_2 (10 mM $NaHCO_3$) on the UV−vis spectrum of CODH at the catalytic redox potentials, $E_d \leq -326$ mV (Table 1) at a time of less than 1 min. Therefore, the increased CO_2 reduction rate (which was measured at a time of 1 min as described in the Materials and Methods and Figure 1) does not correspond to the increased fraction of reduced $[Fe_4S_4]_B$. Furthermore, Nernst analysis of the CO_2 reduction rates over the entire redox range (0 to −530 mV) shows that the E_m for the CO_2 reduction rate is ∼−327 mV for an $n = \sim 1$ process (Figure 1A, trace II). As confirmation of the E_m of this redox-dependent activation process, the CO_2 reduction rates of three additional *batches* of CODH were measured over the redox range of 0 to −530 mV (Figure 1A, inset). The Nernst values (E_m and n) for the redox-dependent activation process of CO_2 reduction from these three additional batches of CODH are identical within 95% confidence limits with average values of $E_m = -329 \pm 6$ mV and of $n = 1.1 \pm 0.2$. The average Nernst values are consistent with the E_m and n values presented in Figure 1A, trace II. The result of Nernst values for the redox-dependent activation process of CO_2 reduction does not correspond to the E_m of $[Fe_4S_4]_B$, −418 mV (*7*, *12*).

The data and analyses indicate that $[Fe_4S_4]_B$ need not be reduced for the catalysis of CO_2 reduction, and that the increase of CO_2 reduction activity cannot be attributed to the increase in reduced FeS_C and $[Fe_4S_4]_B$. Therefore, it is possible to propose that the apparent CO_2 reduction rate is dependent on the redox state of the putative active site, the [FeNi] cluster (*11*). Because CO_2 reduction requires two electrons, it is reasonable to propose that a two-electron reduced state of the active site ($[(CO_L)Fe^{2+}\text{-}Ni^{2+}\text{-}H^-]^{3+}$) is

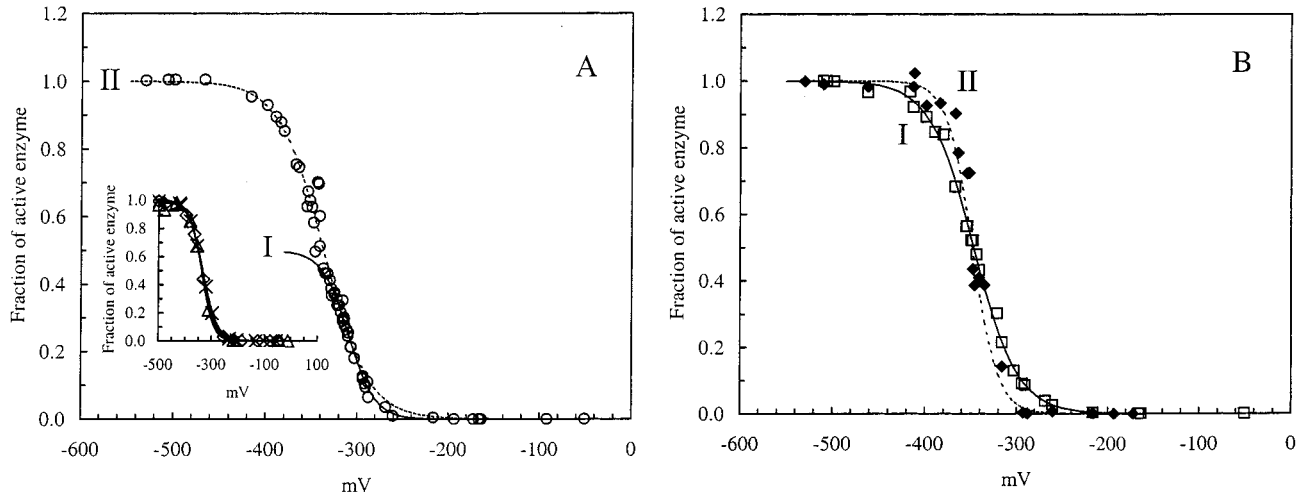

FIGURE 1: Nernst analyses of the CO_2 reduction rate of CODH at various redox states. (A) Assays in the absence of one-electron mediator (○). The assay mixture contained 0.1 mM redox dye, 0.2 mg/mL Hb, 10 mM $NaHCO_3$, and 0.9% NaCl in MOPS buffer (pH 7.5). CO_2 reduction was initiated by adding thionin-oxidized CODH (0.1 μM final concentration) to the assay mixture, and CO_2 reduction rates were monitored for 1 min as described in the Materials and Methods. The assay solutions were adjusted to the desired redox potential by titrations with DTH while monitoring extinction coefficient of each individual dye as described under the Materials and Methods. The maximum activity (V_{max}) for CO_2 reduction in this assay was $(2.3 \times 10^{-1}) \pm (4.2 \times 10^{-2})$ μmol of CO-formed min^{-1} mg of $protein^{-1}$. The measured CO_2 reduction activities at different redox potentials were converted to fractions of active enzyme (γ_a) using eq 2 (V_{max} of DTH-treated sample was set to equal 1). The theoretical curves (I) in the redox range −200 to −340 mV (solid line) and (II) in the redox range 0 to −530 mV (dashed line) were plotted using eq 3, with the flexible Nernst parameters E_m and n. The best fits for the number of electrons involved in the transition (n) were (I) 1.1 ± 0.01 with $E_m = -339 \pm 0.0$ mV ($R^2 = 1.0000$) and (II) 0.9 ± 0.14 with $E_m = -327 \pm 0.3$ mV ($R^2 = 0.9998$). (Inset) Nernst analyses of the CO_2 reduction rate of three additional *batches* of CODH over the potential range 0 to −530 mV. Experimental conditions and procedures are the same as for the main Figure 1A. V_{max} for CO_2 reduction of the three batches of CODH are $(2.1 \times 10^{-1}) \pm (9.1 \times 10^{-2})$ [batch 1 (×)]; $(1.9 \times 10^{-1}) \pm (3.6 \times 10^{-2})$ [batch 2 (◇)]; and $(2.2 \times 10^{-1}) \pm (1.5 \times 10^{-2})$ [batch 3 (□)] μmol of CO-formed min^{-1} mg of $protein^{-1}$. The Nernst analyses for each data set were performed as described above. Results of best fits for the data from the three batches of CODH are $E_m = -336 \pm 0.7$ mV with $n = 1.0 \pm 0.13$ ($R^2 = 0.9999$) for batch 1; $E_m = -328 \pm 2.2$ mV with $n = 1.1 \pm 0.16$ ($R^2 = 0.9999$) for batch 2; and $E_m = -337 \pm 0.5$ mV with $n = 1.0 \pm 0.09$ ($R^2 = 0.9999$) for batch 3. These determined Nernst values were tested using the Student's *t*-statistic and ANOVA (analysis of variance) tests, and produced confidence levels of 95% (*23*). The statistically pooled values of the Nernst values with mean standard deviations are $E_m = -329 \pm 6.4$ mV, with $n = 1.1 \pm 0.28$. (B) Assays in the presence of one-electron mediator (50 μM final concentration). The assay method and assay solution were identical to that of the assay without one-electron mediator except the assay solution contained either methylene blue (MB) or benzyl viologen (BV). The CO_2 reduction activity in the presence of MB (□) was converted to the fraction of active enzyme, and V_{max} was estimated as $(3.1 \times 10^{-1}) \pm (4.0 \times 10^{-2})$ μmol CO-formed min^{-1} mg^{-1} protein. The theoretical curve (I, solid line) was generated as described for Figure 1A. The estimated values of n and E_m using eq 3 were 1.1 ± 0.33 and -348 ± 1.8 mV ($R^2 = 0.9995$). Assays in the presence of BV (◆). BV was added to the assay mixture as described above. The CO_2 reduction activity was converted to the fraction of active enzyme ($\gamma_{a,BV}$) as described previously. The V_{max} was estimated as $(9.4 \pm 5.5) \times 10^{-1}$ μmol CO-formed min^{-1} mg^{-1}. The theoretical curve (II, dashed line) was generated as described above and estimated values of n and E_m using eq 3 were 1.7 ± 0.16 and -347 ± 4.9 mV ($R^2 = 0.9995$).

required for the CO_2 reduction. Furthermore, the observation that no CO_2 reduction occurs at the C_{red1} state [the assigned spin state of $[(CO_L)Fe^{3+}\text{-}Ni^{2+}\text{-}H^-]^{4+}$ (one-electron reduced state) with $FeS_C{}^{1+}$] suggests that no electrons flow from reduced FeS_C to $[(CO_L)Fe^{3+}\text{-}Ni^{2+}\text{-}H^-]^{4+}$ to form $[(CO_L)Fe^{2+}\text{-}Ni^{2+}\text{-}H^-]^{3+}$. This analysis is consistent with our previously published spectroscopic studies, which show that the potential of the $[(CO_L)Fe^{3+}\text{-}Ni^{2+}\text{-}H^-]^{4+}/[(CO_L)Fe^{2+}\text{-}Ni^{2+}\text{-}H^-]^{3+}$ couple is significantly lower than that of $FeS_C{}^{2+/1+}$ (*11*). It is also possible that an unknown redox event occurs in the potential range −295 to −326 mV, and it may cause a ligand shift or induce a different ligand coordination of the metal clusters. In addition, the rate of the CoA/acetyl-CoA exchange from *Clostridium thermoaceticum* CODH is also slow at potentials higher than −400 mV (*17*). By lowering the potential below −400 mV, Lu and Ragsdale observed the exchange rate increases ∼2000-fold and concluded that the highest exchange rate of CoA/acetyl-CoA occurs for fully activated CODH at the lower potential (*17*).

Effect of One-Electron Mediators on the Rate of CO_2 Reduction. The viologens are one-electron accepting redox mediators, in contrast to two-electron dyes used to set the redox potential of the assays. The addition of viologens in the assay mixture has a dramatic stimulatory effect on the rate of CO_2 reduction by CODH at a redox potential of −326 mV and lower (Table 1) (*3*). As seen in Table 1, the addition of 50 μM methyl viologen (MV) or benzyl viologen (BV) to the assays results in up to a 52-fold increase in the rate of CO_2 reduction.

The stimulatory effect of viologens on CO_2 reduction rate can be interpreted as follows: (i) viologens may facilitate the rate at which $[Fe_4S_4]_B{}^{1+}$ reaches redox equilibrium with the surrounding redox buffer and/or (ii) viologens may alter the equilibrium of $[Fe_4S_4]_B{}^{1+}$ with the surrounding redox buffer during CO_2 reduction at $E_d = -326$ mV. The second possibility (that the equilibrium of $[Fe_4S_4]_B{}^{1+}$ with the redox buffer is changed by an addition of viologens at $E_d = -326$ mV) is invalid, because there is no effect of viologens on the fraction of reduced metal clusters (in the absence of substrate) as monitored by UV-absorption spectroscopy (Table 1). Furthermore, if the rate of CO_2 reduction in the presence of excess DTH simply corresponds to the fraction of reduced $[Fe_4S_4]_B$, the rate could not be changed by addition of viologens, because $[Fe_4S_4]_B$ must be fully reduced in the presence of excess DTH. Ensign observed that the rate of CO_2 reduction is enhanced by increasing the amount of BV

and MV even in the presence of a large excess of DTH (*3*). This result supports the first hypothesis and, therefore, suggests that the viologens reduce the time required to establish $[[Fe_4S_4]_B]$/[redox buffer] equilibrium during CO_2 reduction. This analysis suggests that the time required to reach redox equilibrium of $[[Fe_4S_4]_B]$/[redox buffer] in the presence of viologens is much faster than in the absence of viologens. For this reason, the actual rate-limiting step for CO_2 reduction in the absence of viologens could be the time required to establish $[[Fe_4S_4]_B]$/[redox buffer] equilibrium. Similar effects of viologens have been observed for several hydrogenases (*18*, *19*).

Another one-electron mediator, methylene blue (MB), has a much higher potential and is ineffective in stimulating CO_2 reduction. The estimated Nernst value for the CO_2 reduction rate in the presence of MB is $n = \sim 1$ with E_m of ~ -348 mV (Figure 1B, trace I). The values are similar to the Nernst value fitted to the apparent CO_2 reduction rate in the absence of a one-electron mediator (Figure 1A, trace II), suggesting that MB does not stimulate CO_2 reduction of CODH. In combination with the previous study that MB is not a suitable electron acceptor for CO oxidation (*1*), we conclude that MB does not interact with $[Fe_4S_4]_B$ effectively in both CO_2 reduction and CO oxidation. Reasons for the ineffectiveness of MB for either accepting or donating electrons are unclear at this time. However, data indicates that not all one-electron mediators facilitate the redox equilibrium of $[[Fe_4S_4]_B]$/[redox buffer]. Therefore, we conclude that the enhancement of the CO_2 reduction rate of CODH by MV and BV could be viologen-specific but not one-electron-specific. These observations are important because in further studies the stimulatory effects of viologens on activity as a function of potential will need to be considered in any calculations performed using CODHs/ACSs from other organisms. Additionally, while previous studies from our laboratory recognized the stimulatory effect of viologens, a careful examination of the redox dependence of this stimulation was not performed. Further, as the following section will describe, analyses of CODH activity with viologens provides confirmation of the one-electron activation process, with an E_m for CO_2 reduction activity near -339 mV.

Nernst Analyses of the Effects of Viologens on the Redox-Dependent CO_2 Reduction Rate. The effect of viologens over a wide range of redox potentials cannot be analyzed simply because the redox events of viologens also occur in a redox range similar to that for the onset of CO_2 reduction activity. Furthermore, Nernst values for CO_2 reduction activity in the presence of BV and MV are slightly different; in the presence of BV, $n = 1.7 \pm 0.16$ (Figure 1B) and in the presence of MV, $n = 1.5 \pm 0.07$ (data not shown). If the activation of the CO_2 reduction rate corresponds to the amount of reduced BV, the Nernst values of the CO_2 reduction rate in the presence of BV must be compensated by the fraction of the available reduced BV. The fraction of the reduced BV follows the Nernst equation as shown in eq 4.

$$\gamma_{BV} \equiv \frac{[BV_{red}]}{[BV_{red}]+[BV_{ox}]} = \frac{e^{nF(E_{m,BV} - E_d)/RT}}{1 + e^{nF(E_{m,BV} - E_d)/RT}} = \frac{1}{1 + e^{-nF(E_{m,BV} - E_d)/RT}} \quad (4)$$

In this equation, γ_{BV} represents the fraction of the reduced BV at E_d calculated using a midpoint potential of -350 mV for BV ($E_{m,BV}$). A correction for the effect of the reduced BV on the fraction of active enzyme in the presence of BV could be expressed by eq 5

$$R'_o = R_o\gamma_{correct} = \frac{R_{BV}}{C\gamma_{BV}} \quad (5)$$

where R'_o represents the active enzyme for CO_2 reduction in the presence of viologens, R^o equals the maximum activity in the absence of viologens, $\gamma_{correct}$ is the corrected fraction of the active enzyme, R_{BV} represents the observed rate of CO_2 reduction obtained in the presence of BV, and the constant C equals 51 since BV enhances the rate of CO_2 reduction activity by 51-fold (Table 1). After transforming the data using eq 5, Nernst analysis of the CO_2 reduction rate in the presence of BV reveals that the number of electrons involved in the transition from inactive to active enzyme is ~ 1 ($n = 0.9 \pm 0.09$). Furthermore, after transformation the value of E_m obtained from the analysis of $\gamma_{correct}$ is nearly identical to the result obtained in the absence of the one-electron carrier (γ_a). The above interpretation for the variability of n is substantiated by Nernst analysis of CODH in the presence of MV. This analysis shows that the number of electrons leading to the dramatic increase in CO_2 reduction rate in the presence of MV is ~ 1 (0.7 ± 0.04, data not shown). Using the above equations with $E_{m,MV} = -457$ mV, the values for E_m and n for CODH activation are close to those obtained using only the two-electron dyes. As the rate of CO_2 reduction using MV was also increased 52-fold, the apparent values of n and E_m for the data obtained in the presence of viologens (BV and MV) are likely affected by BV and MV. Therefore, the corrected Nernst values support the hypothesis that the transition of inactive to active CODH for the CO_2 reduction is an $n = \sim 1$ transition with E_m of ~ -339 mV.

EPR-Monitored-Redox Titration in the Presence of CO_2. An EPR-monitored-redox titration in the presence of CO_2 was attempted. In the presence of CO_2, the redox potentials of the redox mixture (CODH with several redox buffers) were unstable at $E_d < -310$ mV; after lowering the potential of the reaction mixtures by adding concentrated DTH, the potential reverted to the original potential of ~ -310 mV within 1 min. This result indicates that at potentials lower than -310 mV, CO_2 reduction occurs, and therefore, the reaction mixtures were not redox-equilibrated (at least 0.15 mM of CODH is required to obtain reasonable EPR data). Even when excess redox mediators were applied, CODH in a solution of potential less than ~ -310 mV increased the redox potential in the presence of CO_2. Therefore, it was not possible to perform a redox titration in the presence of CO_2 (i.e., equilibrium conditions are unobtainable).

CONCLUSIONS

Redox Event That Corresponds to the CO_2 Reduction Activity. (i) CODH is not competent for the reduction of CO_2 at redox potentials greater than ~ -300 mV, and therefore the corresponding redox states C_{ox} and C_{red1} of CODH are not involved in the catalysis of CO_2. (ii) The inactive CODH

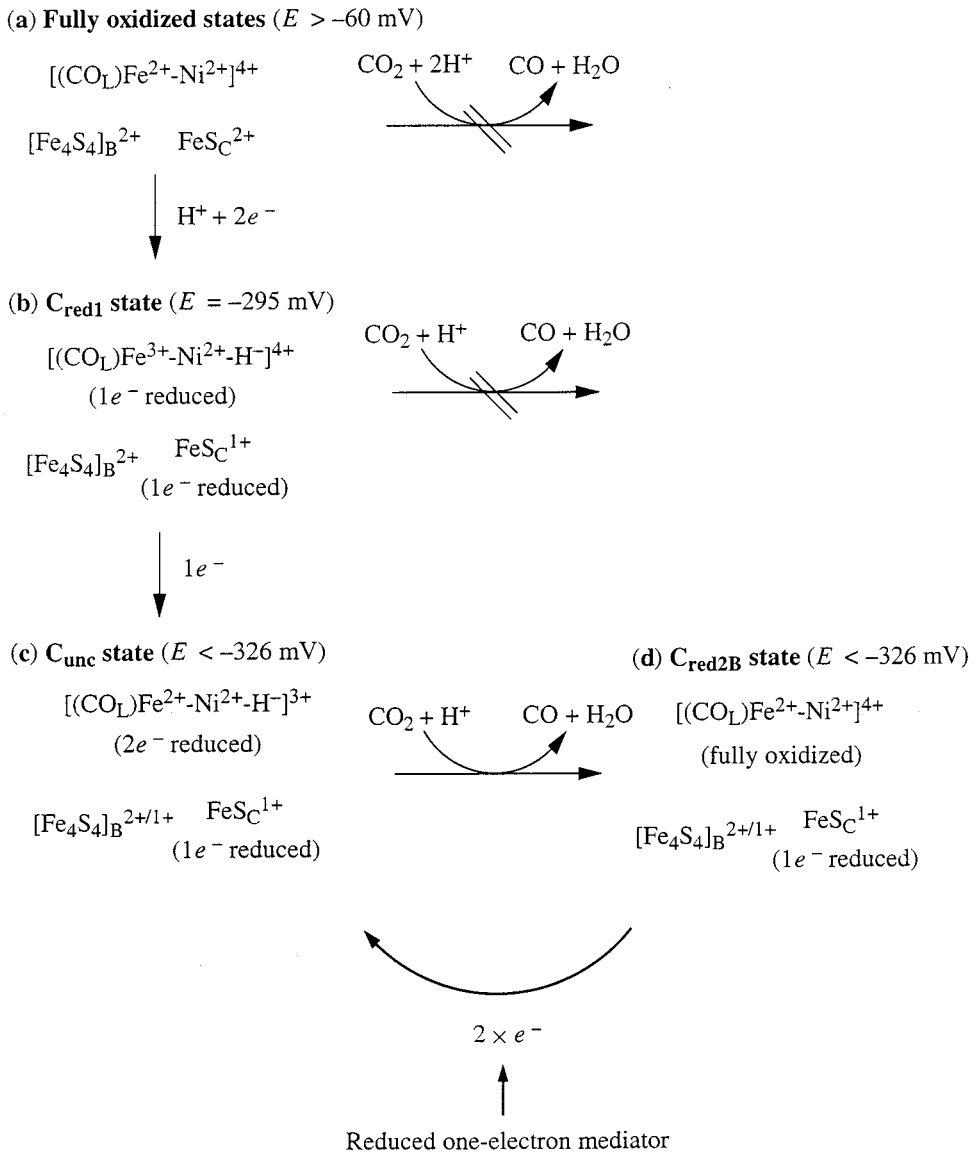

FIGURE 2: Proposed model for the mechanism of CO_2 reduction.

is converted to the catalytically active CODH by lowering the E_d below −300 mV. This potential corresponds directly to the observed shift in the EPR spectrum from C_{red1} to C_{unc} reported previously (*11*). (iii) The activation process involves a one-electron reduction. From these analyses we conclude that the conversion of C_{red1} to C_{unc} is due to a reduction of a one-electron-reduced [FeNi] cluster to a two-electron-reduced [FeNi] cluster:

$$[(CO_L)Fe^{3+}\text{-}Ni^{2+}\text{-}H^-]^{4+} \xrightarrow{1e^-} [(CO_L)Fe^{2+}\text{-}Ni^{2+}\text{-}H^-]^{3+}$$

Effect of Reduced $[Fe_4S_4]_B$ and Viologens on the Rate of CO_2 Reduction Activity. (i) $[Fe_4S_4]_B$ does not need to be fully reduced for CO_2 reduction to occur. However, the presence of reduced $[Fe_4S_4]_B$ does stimulate activity slightly. (ii) Viologens facilitate the rate of CO_2 reduction. The analyses of data suggest that viologens promote a rapid redox equilibrium of $[[Fe_4S_4]_B]$/[redox buffer] which causes an increase in the CO_2 reduction rate. Therefore, the actual rate-limiting step for the CO_2 reduction in the absence of viologens could be the time required to establish an $[[Fe_4S_4]_B]$/[redox buffer] equilibrium.

Proposed Mechanism of CO_2 Reduction. Upon the basis of the above analyses and previous EPR studies (*11*, *20*, *21*), a model for the mechanism of CO_2 reduction can be proposed (Figure 2). In this model, fully oxidized CODH (a) and CODH at the C_{red1} state (b) are unable to reduce CO_2 to CO because the putative [FeNi] cluster is not sufficiently reduced and electron flow from FeS_C^{1+} to the one-electron-reduced [FeNi] cluster does not occur. At the C_{unc} state of CODH (c), the $2e^-$-reduced [FeNi] subcluster catalyzes the reduction of CO_2 to CO and electrons are then passed via $[Fe_4S_4]_B$ and FeS_C to the active site [FeNi] cluster (however, $[Fe_4S_4]_B$ is only partially reduced). Therefore, CO_2 reduction only occurs effectively when the putative [FeNi] subcluster is fully reduced ($[(CO_L)Fe^{2+}\text{-}Ni^{2+}\text{-}H^-]^{3+}$; i.e., the C_{unc} state). The observation of the C_{red2B} signal (defined as the state giving rise to the EPR signal with $g = 1.75$) from the uncoupled state requires CO_2 treatment as shown previously (*11*, *20*, *21*). The production of the C_{red2B} state (d) only occurs after CO_2 reduction by CODH in the C_{unc} state (c). CO is produced in this process; therefore the C_{red2B} state is likely two electrons more oxidized than the C_{unc} state. Note that the C_{unc} state of CODH from *C. thermoaceticum* was also

observed by Fraser et al., although they interpreted the results differently (*22*). When *C. thermoaceticum* CODH was reduced with titanium citrate (Ti-citrate) in the absence of CO_2, the C_{unc} state was present. Addition of CO_2 to the Ti-citrate-reduced CODH sample produced C_{red2B} (*22*).

ACKNOWLEDGMENT

We thank Dr. Gary P. Roberts and Dr. Robert L. Kerby for discussions.

REFERENCES

1. Bonam, D., Murrell, S. A., and Ludden, P. W. (1984) *J. Bacteriol. 159*, 693−699.
2. Bonam, D., and Ludden, P. W. (1987) *J. Biol. Chem. 262*, 2980−2987.
3. Ensign, S. A. (1995) *Biochemistry 34*, 5372−5381.
4. Lindahl, P. A., Münck, E., and Ragsdale, S. W. (1990) *J. Biol. Chem. 265*, 3873−3879.
5. Ragsdale, S. W., Clark, J. E., Ljungdahl, L. G., Lundie, L. L., and Drake, H. L. (1983) *J. Biol. Chem. 258*, 2364−2369.
6. Drennan, C. L., Spangler, N. J., Ludden, P. W., and Rees, D. C. (1998) *FASEB J 12*, 695.
7. Hu, Z., Spangler, N. J., Anderson, M. E., Xia, J., Ludden, P. W., Lindahl, P. A., and Münck, E. (1996) *J. Am. Chem. Soc. 118*, 830−845.
8. Spangler, N. J., Meyers, M. R., Gierke, K. L., Kerby, R. L., Roberts, G. P., and Ludden, P. W. (1998) *J. Biol. Chem. 273*, 4059−4064.
9. Staples, C. R., Heo, J., Spangler, N. J., Kerby, R. L., Roberts, G. P., and Ludden, P. W. (1999) *J. Am. Chem. Soc. 121*, 11034−11044.
10. Ensign, S. A., and Ludden, P. W. (1991) *J. Biol. Chem. 266*, 18395−18403.
11. Heo, J., Staples, C. R., Telser, J., and Ludden, P. W. (1999) *J. Am. Chem. Soc. 121*, 11045−11057.
12. Spangler, N. J., Lindahl, P. A., Bandarian, V., and Ludden, P. W. (1996) *J. Biol. Chem. 271*, 7973−7977.
13. Heo, J., Staples, C. R., Halbleib, C. M., and Ludden, P. W. (2000) *Biochemistry 39*, 7956−7963.
14. Ensign, S. A., Bonam, D., and Ludden, P. W. (1989) *Biochemistry 28*, 4968−4973.
15. Bonam, D., Lehman, L., Roberts, G. P., and Ludden, P. W. (1989) *J. Bacteriol. 171*, 3102−3107.
16. Smith, P. K., Krohn, R. I., Hermanson, G. T., Mallia, A. K., Gartner, F. H., Provenzano, M. D., Fujimoto, E. K., Goeke, N. M., Olson, B. J., and Klenk, D. C. (1985) *Anal. Biochem. 150*, 76−85.
17. Lu, W.-P., and Ragsdale, S. W. (1991) *J. Biol. Chem. 266*, 3554−3564.
18. McTavish, H., Sayavedra-Soto, L. A., and Arp, D. J. (1996) *Biochim. Biophys. Acta 1294*, 183−190.
19. Pershad, H. R., Duff, J. L. C., Heering, H. A., Albracht, S. P. J., and Armstrong, F. A. (1999) *Biochemistry 38*, 8992−8999.
20. Anderson, M. E., and Lindahl, P. A. (1996) *Biochemistry 35*, 8371−8380.
21. Russell, W. K., and Lindahl, P. A. (1998) *Biochemistry 37*, 10016−10026.
22. Fraser, D. M., and Lindahl, P. A. (1999) *Biochemistry 38*, 15706−15711.
23. Zar, J. H. (1984) *Biostatistical Analysis*, 2nd. ed., Prentice Hall, New Jersey.

BI002554K